Genome-wide siRNA screen identifies UNC50 as a regulator of Shiga toxin 2 trafficking

Andrey S. Selyunin,[1,2,3] Lakesla R. Iles,[4] Geoffrey Bartholomeusz,[4] and Somshuvra Mukhopadhyay[1,2,3]

[1]Division of Pharmacology and Toxicology, College of Pharmacy, [2]Institute for Cellular and Molecular Biology, and [3]Institute for Neuroscience, The University of Texas at Austin, Austin, TX
[4]Department of Experimental Therapeutics, MD Anderson Cancer Center, Houston, TX

Shiga toxins 1 and 2 (STx1 and STx2) undergo retrograde trafficking to reach the cytosol. Early endosome-to-Golgi transport allows the toxins to evade degradation in lysosomes. Targeting this trafficking step has therapeutic promise, but the mechanism of trafficking for the more potent toxin STx2 is unclear. To identify host factors required for early endosome-to-Golgi trafficking of STx2, we performed a viability-based genome-wide siRNA screen in HeLa cells. 564, 535, and 196 genes were found to be required for toxicity induced by STx1 only, STx2 only, and both toxins, respectively. We focused on validating endosome/Golgi-localized hits specific for STx2 and found that depletion of UNC50 blocked early endosome-to-Golgi trafficking and induced lysosomal degradation of STx2. UNC50 acted by recruiting GBF1, an ADP ribosylation factor–guanine nucleotide exchange factor (ARF-GEF), to the Golgi. These results provide new information about STx2 trafficking mechanisms and may advance efforts to generate therapeutically viable toxin-trafficking inhibitors.

Introduction

Shiga toxin (STx), produced by *Shigella*, and the closely related STx type 1 (STx1) and type 2 (STx2), produced by strains of STx-producing *Escherichia coli* (STEC), are lethal bacterial exotoxins that belong to the AB_5 class (Beddoe et al., 2010; Mukhopadhyay and Linstedt, 2013). These toxins are formed by the association of a single A subunit with a pentameric B subunit (Beddoe et al., 2010; Mukhopadhyay and Linstedt, 2013). STx and STx1 are nearly identical; the only difference is a conservative serine-to-threonine substitution in the A subunit (Strockbine et al., 1988; Mukhopadhyay and Linstedt, 2013). In contrast, STx2 shares only ∼55% sequence identity with STx and STx1 (Strockbine et al., 1988; Mukhopadhyay and Linstedt, 2013). The toxins kill cells by blocking protein synthesis in the cytosol; the mechanism is the removal by the A subunit of a specific adenine residue in the 28S rRNA of the 60S ribosome (Beddoe et al., 2010; Mukhopadhyay and Linstedt, 2013). Although the A subunit is catalytically active, it cannot traffic to the cytosol of target cells by itself. Instead, trafficking is mediated by the pentameric B subunits (Mukhopadhyay and Linstedt, 2013). Interestingly, infections caused by STx-producing *Shigella* can be treated with antibiotics (Ochoa and Cleary, 2006). However, in patients infected with STEC, usage of at least some classes of antibiotics increases production of STx1 and STx2 and enhances the risk of developing life-threatening complications such as hemolytic uremic syndrome (Walterspiel et al., 1992; Matsushiro et al., 1999; Zhang et al., 2000; McGannon et al., 2010). Consequently, for STEC infections, antibiotic usage is contraindicated, and there are no definitive therapies (Nataro, 2006).

As cytosolic translocation of the A subunits is a prerequisite for toxicity, blocking toxin trafficking is an attractive therapeutic strategy. Inhibitors that alter trafficking and toxicity of STx1 and/or STx2 have been identified (Saenz et al., 2007; Stechmann et al., 2010; Mukhopadhyay and Linstedt, 2012, 2013; Kavaliauskiene et al., 2017), but none are approved for use in humans. For success in humans, an inhibitor must ideally target toxin trafficking but not affect levels or localization of host proteins. Additionally, inhibitors must effectively block STx2 because the in vivo LD_{50} of STx2 is ∼400 times lower than that of STx1 (Tesh et al., 1993), and in humans, disease severity correlates with STx2 production (Boerlin et al., 1999). Securing a comprehensive understanding of the mechanisms by which STx1 and STx2 traffic through host cells is likely to aid in the rational design of transport inhibitors that exclusively inhibit toxin transport without impacting host proteins.

Although STx2 is more disease-relevant, most of our current understanding of toxin trafficking comes from work on STx1. Trafficking starts with the association of the B subunit of STx1 (STx1B) with the glycosphingolipid globotriaosylceramide on the cell surface (Beddoe et al., 2010; Mukhopadhyay

Correspondence to Somshuvra Mukhopadhyay: som@austin.utexas.edu

Abbreviations used: ARF, ADP ribosylation factor; GEF, guanine nucleotide exchange factor; HA, hemagglutinin; STEC, STx-producing *Escherichia coli*; STx, Shiga toxin.

The Rockefeller University Press
J. Cell Biol. Vol. 216 No. 10 3249–3262
https://doi.org/10.1083/jcb.201704015

and Linstedt, 2013). After endocytosis, the toxin sequentially traffics through early endosomes and the Golgi apparatus and is then delivered to the endoplasmic reticulum, from where the A subunit is translocated to the cytosol (Mukhopadhyay and Linstedt, 2013). A particularly critical step is direct transit from early endosomes to the Golgi apparatus, which allows the toxin to bypass late endosomes/lysosomes where degradative proteolytic enzymes are active (Mallard et al., 1998; Mukhopadhyay and Linstedt, 2013). The direct early endosome-to-Golgi transport step is mediated by the host protein GPP130 (Natarajan and Linstedt, 2004; Mukhopadhyay and Linstedt, 2012, 2013; Mukhopadhyay et al., 2013). GPP130 is a single-pass transmembrane protein that constitutively cycles between the Golgi apparatus and early endosomes (Linstedt et al., 1997; Bachert et al., 2001). STx1B directly binds GPP130 (K_d = 150 nM), which allows the toxin to "piggyback" on GPP130 and traffic to the Golgi from early endosomes (Mukhopadhyay and Linstedt, 2012, 2013; Mukhopadhyay et al., 2013). In the absence of GPP130, STx1B still reaches early endosomes but then fails to traffic to the Golgi and is rerouted to lysosomes for degradation (Mukhopadhyay and Linstedt, 2012, 2013). Thus, GPP130 acts as the endosomal receptor for STx1B. Importantly, exposure of cells to low doses of the essential metal manganese induces rapid degradation of GPP130 (Mukhopadhyay et al., 2010; Mukhopadhyay and Linstedt, 2011, 2012; Tewari et al., 2014, 2015). Treatment with manganese provides 3,800-fold protection against STx1-induced death in cell culture and 100% protection against STx1-induced lethality in mice (Mukhopadhyay and Linstedt, 2012). An important implication is that targeting the early endosome-to-Golgi step is an effective means to block STx1 transport and protect against toxin-induced disease.

Over the last few years, we focused on delineating the mechanisms of trafficking of STx2. Our previously published work shows that, similar to STx1, STx2 also undergoes direct early endosome-to-Golgi trafficking (Selyunin and Mukhopadhyay, 2015). However, there are important molecular differences. The B subunit of STx2 (STx2B) does not bind GPP130, and consequently, trafficking of STx2 is GPP130 independent and manganese insensitive (Mukhopadhyay et al., 2013). Despite this, both toxins use a conserved structural motif (the surface-exposed β4–β5 loop of the B subunit) to sort out of early endosomes and traffic to the Golgi (Mukhopadhyay et al., 2013; Selyunin and Mukhopadhyay, 2015); the β4–β5 loop of STx1B mediates interaction with GPP130, whereas that of STx2B does not (Mukhopadhyay et al., 2013). These thematic similarities raise the possibility that an as yet undiscovered endosomal receptor may mediate early endosome-to-Golgi transport of STx2B. Conceptual similarities with STx1 also suggest that targeting early endosome-to-Golgi transport of STx2 may protect against lethal toxicosis. Consistent with this, mutations in STx2B that block endosome-to-Golgi transport induce lysosomal degradation of the toxin (Selyunin and Mukhopadhyay, 2015).

Based on this reasoning, a major goal of our research group is to identify host factors that are required for the early endosome-to-Golgi transit of STx2 and subsequently elucidate the molecular mechanisms. To achieve this in an unbiased manner, we performed in this study a viability-based genome-wide siRNA screen in HeLa cells and sought to identify genes that were required for STx2-induced toxicity; we used STx1 as control in the screen. An imaging-based screen that directly assayed for STx2B transport would be ideal, but presented insurmountable technical hurdles. The screen identified 535 genes that were only required for toxicity induced by STx2, 564 that were only required for toxicity induced by STx1, and 196 that were required for both toxins. Validation and characterization assays focused on STx2 hits predicted to localize to endosomes/Golgi. Through these studies, we discovered that UNC50 mediated early endosome-to-Golgi transport of STx2 by recruiting GBF1, an ADP ribosylation factor (ARF)-guanine nucleotide exchange factor (GEF), to the Golgi. Overall, results presented in this study provide fundamental insights into the mechanisms by which STx1 and STx2 exploit host trafficking pathways to intoxicate cells, improve understanding of the mechanisms of protein trafficking at the endosome/Golgi interface in eukaryotic cells, and may aid in the development of a treatment for STEC-induced disease.

Results

High-throughput viability-based genome-wide siRNA screen

To identify factors required for trafficking and toxicity of STx2, we used a viability-based genome-wide siRNA screening approach. We performed the screen in HeLa cells and used a human genome-wide siRNA library, which comprised pooled siRNAs targeting 21,067 predicted open reading frames such that each gene was simultaneously targeted by four separate siRNAs. In brief, cells were reverse transfected with pooled siRNAs, exposed to 0.1 pg/ml STx2 or 0.4 pg/ml STx1 (STx1 was used as control), and then viability was assessed (see the Primary genome-wide siRNA screen... section of Materials and methods for details). The concentration of each toxin was its LD_{50} in our cell line. For each toxin, we performed the screen in triplicate. Primary hits were genes for which viability was two SDs greater than the mean viability of all genes in that screen (i.e., z score >2; see the Primary genome-wide siRNA screen… section of Materials and methods for detailed statistical methodology). We obtained 760 primary hits in the STx1 screen and 731 in the STx2 screen (Tables S1 and S2). Of these, 564 primary hits were unique for STx1 (these did not impact STx2), 535 were unique for STx2 (these did not impact STx1), and 196 were common for both toxins (Table S3). The screen was largely successful as it identified genes known to be required for the trafficking of STx1B as hits in the STx1 part of the study (e.g., Ykt6, the conserved oligomeric Golgi complex, Rab6a, and Rab43; Zolov and Lupashin, 2005; Fuchs et al., 2007; Mukhopadhyay and Linstedt, 2013).

Gene ontology analyses revealed that primary screen hits had diverse functions (Fig. 1 A). For further studies, we classified hits based on predicted intracellular localization. 18 STx1-unique, 35 STx2-unique, and 14 common hits were predicted to localize to endosomes/Golgi (Fig. 1 B and Table S4). We focused on STx2-unique hits predicted to localize to endosomes/Golgi because these were most likely to have a specific impact on endosome-to-Golgi transport of STx2. To rule out false positives, we processed these hits through a secondary screen. For this, (A) the siRNA pool was deconvoluted, (B) each hit was independently targeted with four separate siRNAs, (C) each knockdown was performed at least in triplicate, (D) after knockdown, similar to the primary screen, cells were exposed to 0.1 pg/ml STx2 (LD_{50} of STx2), and then (E) viability was assessed (see the Secondary screen and data analysis section of Materials and methods for details). In the primary STx2 screen

after knockdown and toxin treatment, mean normalized viability of all genes assayed was 42% with an SD of 10%; therefore, viability of hits was >62% (z score >2; Table S2). In order for a primary screen hit to be considered as validated in the secondary screen, its normalized viability after knockdown with least two of the four individual siRNAs and after STx2 exposure had to be >62% (Fig. 1 C and Table S5; see the Secondary screen and data analysis section of Materials and methods for details of data analyses). The secondary screen validated five hits; of these, three hits were validated with three siRNAs (UNC50, β-1,4-galactosyltransferase 5, and fucosyltransferase 1), two hits were validated with two siRNAs (kinase insert domain receptor and sorting nexin 14). A further seven hits gave reproducible results with one siRNA (signal transducing adapter molecule, two-pore segment channel 1, sorting nexin 1, astrotactin 2, ATPase phospholipid transporting 11 A, adapter-related protein complex 1 associated regulatory protein, and Rab2a; Fig. 1 C and Table S5).

After this, we performed detailed functional analyses on one validated hit, UNC50, for the following reasons: As described in the previous paragraph, three hits, UNC50, β-1,4-galactosyltransferase 5, and fucosyltransferase 1 were validated using three separate siRNAs in the secondary screen (Fig. 1 C and Table S5). A direct implication was that these hits may be crucially important for STx2 cytotoxicity. Of these, at least one siRNA targeting UNC50 or β-1,4-galactosyltransferase 5, but not fucosyltransferase 1, provided complete protection against STx2-induced cell death (Fig. 1 C and Table S5); therefore, we decided to focus on fucosyltransferase 1 at a later time. β-1,4-galactosyltransferase 5 functions as a lactosylceramide synthase enzyme (Tokuda et al., 2013). Lactosylceramide is a necessary precursor for synthesis of globotriaosylceramide, the cell surface glycosphingolipid receptor of STx1 and STx2 (Beddoe et al., 2010; Tokuda et al., 2013). Preliminary assays revealed that depletion of β-1,4-galactosyltransferase 5 reduced globotriaosylceramide levels and blocked the binding of STx2B to the cell surface, providing a straightforward explanation for the requirement of β-1,4-galactosyltransferase 5. In contrast, the mechanism of action of UNC50 was unclear, but there was a possibility that it may function as the endosomal receptor for STx2B. Analogy with the GPP130-STx1B paradigm suggested that the putative STx2B endosomal receptor may be a transmembrane protein that localized to endosomes/Golgi and specifically influenced trafficking and toxicity of STx2 but not STx1. UNC50 fulfilled these broad criteria because prior studies localized it to the Golgi apparatus and indicated that it contained five transmembrane domains (Chantalat et al., 2003; Eimer et al., 2007). Furthermore, depletion of UNC50 did not protect against STx1-induced cell death in the primary screen (STx1 z score = 0.5; Table S1). As the overarching hypothesis driving this line of research was that an endosomal receptor may mediate STx2B transport, UNC50 was a logical choice for mechanistic assessment.

Generation of a ΔUNC50 cell line

To elucidate the mechanisms by which loss of UNC50 protected against STx2, we generated a stable HeLa cell subline in which UNC50 was depleted using a lentivirus-based CRISPR system. As noted in the previous section, UNC50 is predicted to have five transmembrane domains (Fig. 2 A; Chantalat et al., 2003; Eimer et al., 2007). Sequencing of genomic DNA revealed that in our *ΔUNC50* cell line, stop codons were introduced in or immediately after the region coding for the second transmembrane domain (Fig. 2 B). There were two separate mutations (Fig. 2 B), which likely corresponded with independent changes introduced in two chromosomes. These mutations were expected to reduce UNC50 mRNA and protein levels and inactivate function. For validation, we performed RT-PCR analyses. We ran two separate reactions designed to amplify products from regions upstream or downstream of the introduced stop codons. In WT cells, a positive product was detected for both reactions (Fig. 2 C). Importantly, however, in *ΔUNC50* cells, a positive product was generated for the upstream but not the downstream reaction (Fig. 2 C), suggesting that the introduced stop codons effectively terminated transcription. Unfortunately, we could not verify loss of endogenous UNC50 protein because we could not identify a commercial antibody that specifically detected UNC50 in human cell lines. As another approach to validate protein loss, we used transient transfection and overexpressed CRISPR-sensitive or CRISPR-resistant full-length myc-tagged UNC50 in WT or *ΔUNC50* cells. 1 d after transfection, compared with WT cells, levels of CRISPR-sensitive myc-UNC50 were substantially lower in *ΔUNC50* cells (Fig. 2, D and E). The reduced expression was not evident for a control construct, GFP-tagged SLC30A10, and more importantly, for CRISPR-resistant myc-tagged UNC50 (for reasons that are unclear, expression of CRISPR-resistant myc-tagged UNC50 was greater in *ΔUNC50* cells; Fig. 2, D–G). These results suggest that the CRISPR system specifically reduced UNC50 expression in *ΔUNC50* cells. The expression of limited amounts of UNC50 protein from the CRISPR-sensitive construct in *ΔUNC50* cells may be because of several reasons, such as high plasmid copy number per cell or introduction of mutations in the plasmid that were different from the in-frame stop codons inserted in genomic DNA. Additionally, 1 d after transfection, CRISPR-sensitive myc-UNC50 primarily localized to the endoplasmic reticulum in WT cells, but in *ΔUNC50* cells, it was enriched in the Golgi (Fig. 2, H–J). Prior research in yeast demonstrated that hemagglutinin (HA)-tagged endogenous UNC50 was enriched in the Golgi, but when UNC50 was overexpressed from a multicopy plasmid, it accumulated in the endoplasmic reticulum (Chantalat et al., 2003). For our data, it was likely that the relatively low expression of CRISPR-sensitive myc-UNC50 in *ΔUNC50* cells allowed the protein to traffic to the Golgi and attain a localization resembling that of endogenous UNC50. The Golgi localization of myc-UNC50 in *ΔUNC50* cells was useful for rescue experiments described in Figs. 3 (J–L) and 4 (L–O). Overall, results in Fig. 2 suggest that UNC50 is effectively depleted in *ΔUNC50* cells.

UNC50 is required for the trafficking of STx2B from early endosomes to the Golgi

After this, we sought to determine the mechanism by which depletion of UNC50 protected against STx2-induced cell death. As the first step, we validated that protection against STx2 toxicity was evident in *ΔUNC50* cells. The LD_{50} of STx2 in *ΔUNC50* cells (5.7 pM) was ∼200-fold greater than that in WT cells (0.03 pM), confirming robust protection (Fig. 3, A and B). To elucidate the underlying mechanism, we tested whether trafficking of STx2 was altered in *ΔUNC50* cells. For this, we assayed for the trafficking of STx2B in WT and *ΔUNC50* cells. Consistent with our prior work (Selyunin and Mukhopadhyay, 2015), in WT cells, STx2B bound the cell surface at the start of the assay and was clearly detected in the Golgi at the 60-min

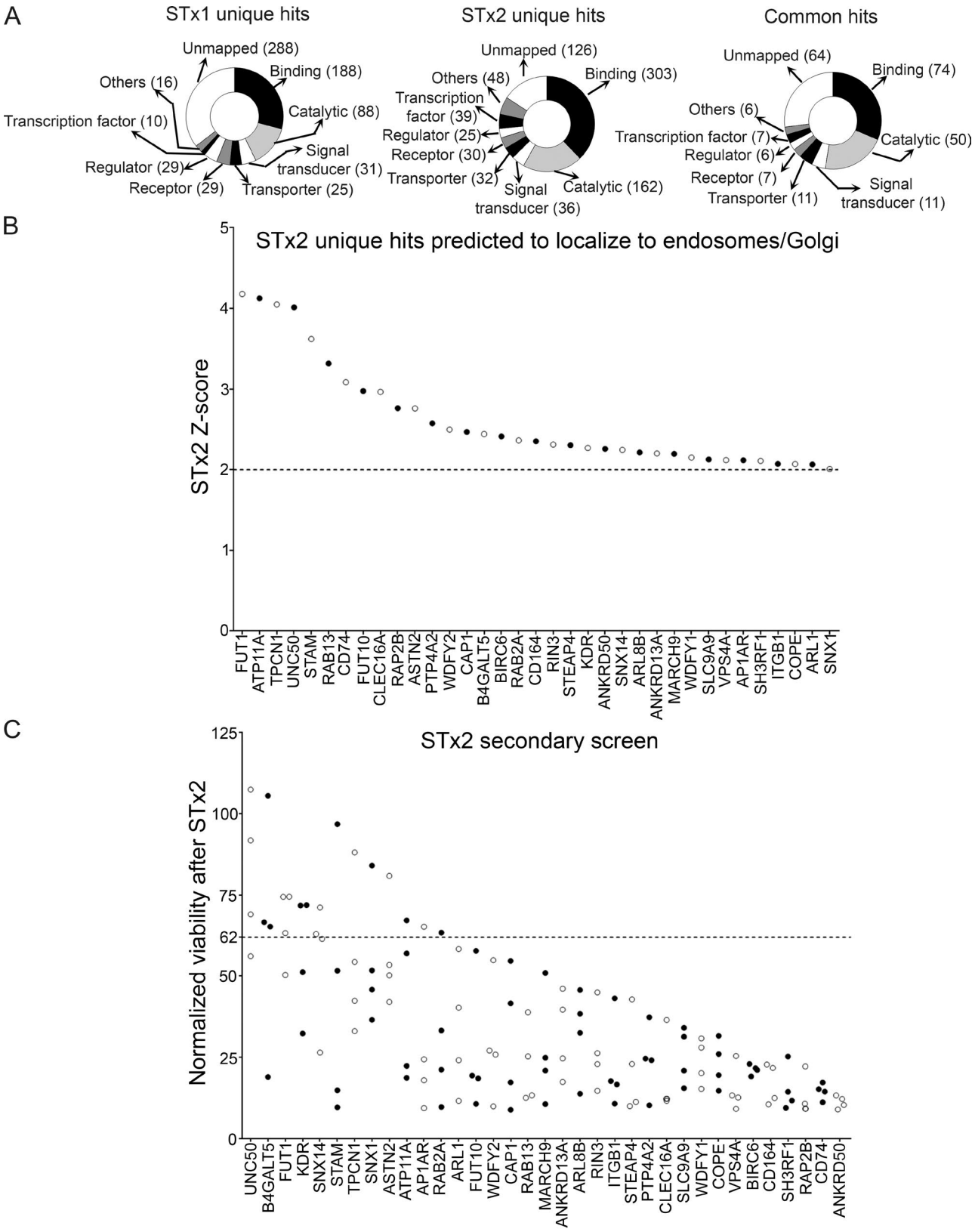

Figure 1. **Classification and analyses of hits obtained in the primary and secondary siRNA screens.** (A) Schematic illustrating annotated functions of hits identified in the primary genome-wide siRNA screen. Functions were retrieved from the universal protein resource database (UniProt). Note that one gene can have multiple annotated functions; therefore, numbers here do not match those provided in the supplemental tables. (B) Graph depicting hits that were unique to STx2 in the primary screen and predicted to localize to endosomes/Golgi. (C) Secondary screen data. Each gene was targeted with four separate siRNAs.

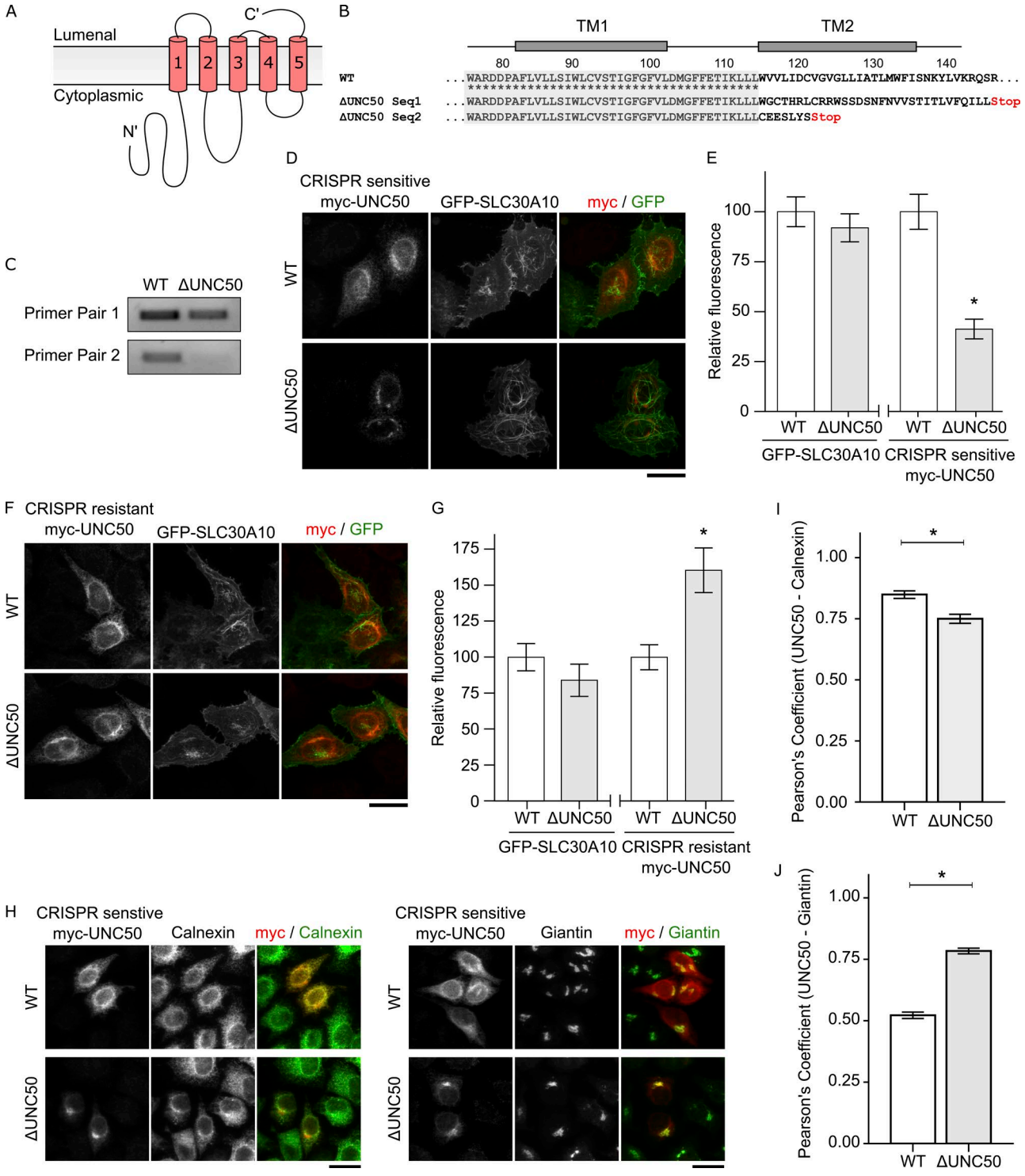

Figure 2. **Generation of *ΔUNC50* HeLa cells.** (A) Schematic of the UNC50 protein with predicted topology. (B) Amino acid sequence of UNC50 in WT and *ΔUNC50* cells. Shaded area with asterisks shows alignment between WT and *ΔUNC50* cells. seq., sequence; TM, transmembrane domain. (C) RT-PCR analyses to detect expression of UNC50 in WT and *ΔUNC50* cells. As described in the RT-PCR section of Materials and methods, primer pairs 1 and 2 were used to amplify sequences upstream or downstream, respectively, of the locus targeted by the CRISPR system. (D) WT or *ΔUNC50* cells were cotransfected with CRISPR-sensitive myc-tagged UNC50 and GFP-tagged SLC30A10. 1 d after transfection, cultures were processed for immunofluorescence. The myc tag was detected using a monoclonal antibody. (E) Quantification of fluorescence intensities from D. For each construct, intensity in WT cells was normalized to 100, and intensity in *ΔUNC50* cells was expressed relative to WT ($n \geq 15$ cells per condition). (F) Immunofluorescence analyses were performed in WT or *ΔUNC50* cells cotransfected with indicated constructs as described in D. (G) Quantification of fluorescence intensities from F as described for E ($n = 15$ cells per condition). (H) WT or *ΔUNC50* cells were transfected with myc-tagged CRISPR-sensitive UNC50. 1 d after transfection, cultures were processed for immunofluorescence. A monoclonal antibody was used to detect the myc tag. Polyclonal antibodies were used to detect the endoplasmic reticulum marker calnexin or the Golgi marker giantin. Bars, 25 µm. (I and J) Quantification of the Pearson's coefficient for colocalization between UNC50 and calnexin or giantin from H ($n \geq 15$ cells per group). *, $P < 0.05$ by *t* test; error bars show means ± SEM).

time point (Fig. 3, C–E). In *ΔUNC50* cells, STx2B also robustly bound the cell surface (Fig. 3 C) and was internalized to early endosomes at the 10-min time point (Fig. 3 F). Importantly, however, the toxin failed to traffic to the Golgi (Fig. 3, C–E). Instead, at the 60-min time point, there was a substantial reduction in the fluorescence intensity of STx2B, and residual toxin was detected in punctate cytoplasmic structures resembling endosomes/lysosomes (Fig. 3, C–E). This finding suggested that STx2B may be undergoing lysosomal degradation in *ΔUNC50* cells. To test this, we pretreated *ΔUNC50* cells with the lysosomal protease inhibitors leupeptin and pepstatin and allowed STx2B to undergo retrograde trafficking for 4 h. Under these conditions, the toxin still did not traffic to the Golgi, but instead of being degraded, it persisted in large punctate structures that partially overlapped with the lysosomal marker Lamp2 (Fig. 3, G–I). Collectively, these results imply that in *ΔUNC50* cells, the early endosome-to-Golgi trafficking of STx2B is inhibited, and the toxin is rerouted to lysosomes for degradation.

To confirm that the block in trafficking was caused by depletion of UNC50, we overexpressed CRISPR-sensitive full-length myc-UNC50 in *ΔUNC50* cells and, 1 d after transfection, assayed for STx2B trafficking. As described in the previous section, in *ΔUNC50* cells 24 h after transfection, myc-UNC50 was enriched in the Golgi (Fig. 2, H–J). Importantly, expression of myc-UNC50 inhibited the degradation of STx2B and rescued its trafficking to the Golgi (Fig. 3, J–L). Thus, UNC50 is required for the early endosome-to-Golgi trafficking of STx2B.

UNC50 is required for optimal transport of GPP130 and STx1B to the Golgi

To determine whether the effect on STx2 transport and toxicity was specific, we performed assays with STx1. This was important because in the genome-wide screen, incomplete knockdown of UNC50 may have led to the lack of protection against STx1 toxicity. Surprisingly, the LD_{50} of STx1 in *ΔUNC50* cells (10.8 pM) was ∼10-fold greater than that in WT cells (0.85 pM; Fig. 4, A and B). Although the protection factor for STx2 (∼200) was an order of magnitude greater than that for STx1 (∼10), these data raised the possibility that UNC50 may play a role in the trafficking of STx1B. To investigate this further, we assayed for the trafficking of STx1B. Colocalization analyses revealed that unlike STx2B, trafficking of STx1B to the Golgi in *ΔUNC50* cells was only modestly less than that in WT cells (Fig. 4, C and D). However, similar to STx2B, in *ΔUNC50* cells, total fluorescence of STx1B at the 60-min time point was substantially lower than that at the start of the assay (Fig. 4 E). Pretreatment with leupeptin and pepstatin increased intracellular STx1B levels in *ΔUNC50* cells; under these conditions, a pool of STx1B was detected in large cytoplasmic punctae resembling lysosomes (Fig. 4, F and G). These results suggest that, in *ΔUNC50* cells, a fraction of internalized STx1B fails to traffic to the Golgi and instead undergoes lysosomal degradation.

To determine the mechanism, we assayed for changes in GPP130, the endosomal STx1B receptor. Compared with WT cells, levels of GPP130 were reduced by ∼75% in *ΔUNC50* cells (Fig. 4, H and I). Treatment of *ΔUNC50* cells with leupeptin and pepstatin led to the accumulation of GPP130 in large cytoplasmic punctae and increased cellular GPP130 levels (Fig. 4, J and K), suggesting that similar to STx1B, a fraction of GPP130 also underwent lysosomal degradation. Expression of CRISPR-sensitive full-length myc-UNC50 in *ΔUNC50* cells rescued levels of GPP130 and STx1B (Fig. 4, L–O), implying that the observed lysosomal degradation of GPP130 and STx1B was caused by loss of UNC50 and not a consequence of nonspecific effects. Collectively, although UNC50 is obligatorily required for the early endosome-to-Golgi transport of STx2B, it is also required for the optimal trafficking of STx1B to the Golgi.

UNC50 mediates STx2B trafficking by recruiting the ARF-GEF GBF1 to the Golgi apparatus

As depletion of UNC50 affected trafficking of multiple cargoes, it was unlikely to be the elusive endosomal receptor for STx2B. Yeast UNC50 directly interacts with the yeast ARF-GEFs Gea1p and Gea2p, human UNC50 also interacts with yeast Gea1p, and depletion of UNC50 in yeast leads to a reduction in the association of Gea2p with membranes (Chantalat et al., 2003). These results suggest that the function of human UNC50 may be to recruit an ARF-GEF to membranes. The human homologue of Gea1/2, GBF1, predominantly localizes to the endoplasmic reticulum–Golgi intermediate compartment and the Golgi apparatus, where it recruits ARF1 to initiate COPI vesicle formation (Szul et al., 2007; Manolea et al., 2008; Donaldson and Jackson, 2011; Lowery et al., 2013; Jackson and Bouvet, 2014). Thus far, GBF1 has not been detected on endosomes. The localization of both UNC50 and GBF1 to the secretory pathway implies that a simple model in which UNC50 mediates endosome-to-Golgi transport of STx2B by directly recruiting GBF1 to endosomal membranes is unlikely to be valid. Importantly, however, GBF1 can be detected in the trans-Golgi network, and activity of GBF1 influences membrane recruitment of trans-Golgi network–localized clathrin adapters and ARF-GEFs (GGA2, AP1, BIG1, and BIG2; Lowery et al., 2013). Furthermore, AP1 and BIG2 also localize to endosomes (Bonifacino, 2004; Shin et al., 2004; Shen et al., 2006), providing a means for changes in GBF1 levels or activity to indirectly influence endosome-to-Golgi transport. Consistent with this, prior work shows that exposure of cells to a small molecule inhibitor of GBF1, golgicide A, blocks endosome-to-Golgi transport of STx1 (Sáenz et al., 2009). Additionally, activity of ARF1, a GBF1 substrate, is required for the endosome-to-Golgi transport of STx1 (Shiba et al., 2010). Based on these data, we hypothesized that the function of UNC50 may be to recruit GBF1 to the Golgi apparatus and that the block in endosome-to-Golgi transport of STx2 observed in *ΔUNC50* cells may be caused by an indirect effect of a decrease in the recruitment of GBF1 to the Golgi.

To test this hypothesis, we first sought to determine whether GBF1 was required for the retrograde trafficking of STx2B. For this, we used a previously characterized siRNA to deplete GBF1 in WT HeLa cells (Szul et al., 2007). Loss of GBF1 induces tubulation of the cis-Golgi, which can be detected by staining for the cis-Golgi marker GM130 (Szul et al., 2007; Lowery et al., 2013). We verified that the anti-GBF1 siRNA robustly reduced GBF1 protein levels and induced GM130 tubulation (Fig. 5, A and B). We then assayed for the transport of STx2B in cells transfected with control or anti-GBF1 siRNAs. In these experiments, we used tubulation of GM130 to detect GBF1-depleted cells because antibodies used to detect GBF1 and STx2B were both raised in rabbits. Importantly, in GBF1-depleted cells, STx2B failed to traffic to the Golgi and instead was trapped in endosome-like punctate structures (Fig. 5, C and D). Thus, GBF1 is required for the trafficking of STx2B to the Golgi. After this, we used immunofluorescence to determine whether tubulation of the Golgi was detectable in

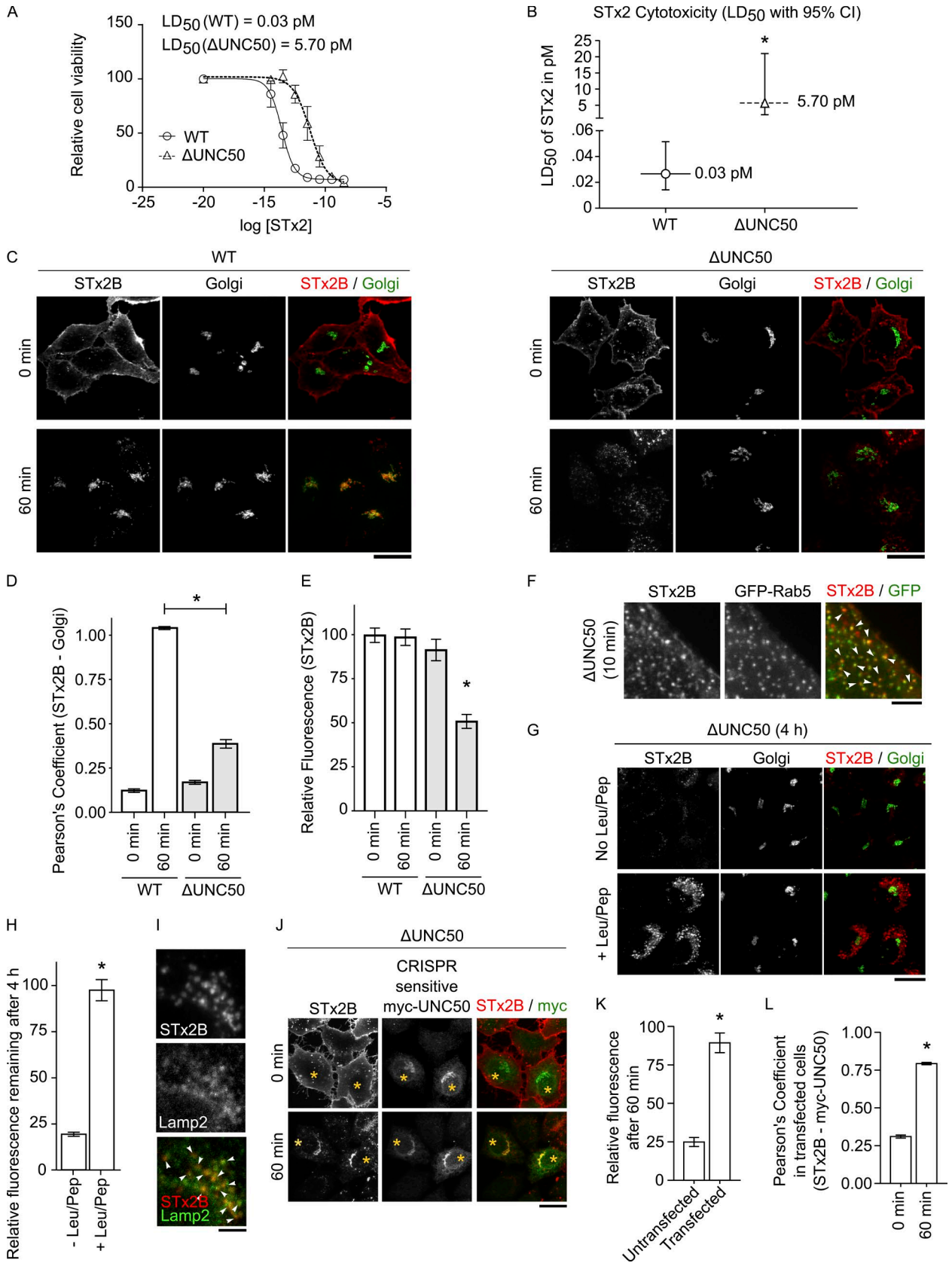

Figure 3. **UNC50 is required for the early endosome-to-Golgi trafficking of STx2.** (A) WT or *ΔUNC50* cells were treated with indicated amounts of STx2 holotoxin for 16 h. Cell viability was then assessed using the MTT assay described in the Viability assays section of Materials and methods. Viability without toxin exposure was normalized to 100 for each cell line ($n = 3$). (B) Depiction of the mean LD_{50} of STx2 from A. Error bars represent 95% confidence intervals (CIs). *, $P < 0.05$ by *t* test. (C) Trafficking of His-tagged STx2B was assayed in WT or *ΔUNC50* cells. Cells were fixed at 0 or 60 min after start of transport. STx2B was detected using a polyclonal antibody against the His tag. Golgi was demarcated using a monoclonal antibody

ΔUNC50 cells. Importantly, staining for GM130 provided clear evidence of Golgi tubulation in *ΔUNC50* cells (Fig. 5 E). Thus, with regard to Golgi structure and retrograde STx2 transport, loss of GBF1 phenocopies that of UNC50. Next, we tested whether loss of UNC50 affected localization and/or levels of GBF1. Compared with WT HeLa cells, there was a decrease in the amount of Golgi-localized GBF1 in *ΔUNC50* cells (Fig. 5, E–G). This decrease was specific to the Golgi because, in comparison with WT cells, total cellular GBF1 levels of *ΔUNC50* cells were similar, whereas levels of non-Golgi GBF1 were greater (Fig. 5, E–G). Furthermore, overexpression of CRI SPR-sensitive myc-UNC50 in *ΔUNC50* cells, which rescued STx2B trafficking (Fig. 3, J–L), also rescued the recruitment of GBF1 to the Golgi (Fig. 5, H–J). Thus, UNC50 is required for the optimal recruitment of GBF1 to the Golgi apparatus. Finally, we analyzed whether ARF1 was required for STx2B trafficking. Overexpression of a dominant-negative version of ARF1 disrupted the Golgi apparatus (Fig. 5 K) consistent with prior work (Shiba et al., 2010). Importantly, in transfected cells, STx2B failed to traffic to the disrupted Golgi elements (Fig. 5, K and L). Thus, activity of ARF1 is required for the transport of STx2B to the Golgi. In sum, data in Fig. 5 are consistent with the model that UNC50 regulates endosome-to-Golgi trafficking of STx2B by recruiting GBF1 to the Golgi apparatus.

Discussion

High-throughput genome-wide knockdown screens are a powerful tool to identify host factors required for the trafficking and cytotoxicity of bacterial and plant toxins. Such screens have previously been performed for ricin and pseudomonas exotoxin (Moreau et al., 2011; Bassik et al., 2013). We now provide data for STx1 and STx2. Three important issues are worth discussing about this approach. First, an inherent drawback of genome-wide screens is that knockdown efficiency is not verified for individual genes, and incomplete knockdown may prevent identification of a required factor. Indeed, in this study, we did not identify GPP130 as a primary hit in the STx1 screen, implying that our screen did not saturate. Similarly, Moreau et al. (2011) did not identify genes encoding the conserved oligomeric Golgi complex as required for ricin toxicity, although other experiments indicated that this complex was required. Despite the lack of saturation, the strength of the screening approach is in identifying hits that protect against toxicity. As described in the first section of the Results, we identified factors previously known to be required for STx1 trafficking as hits in the STx1 primary screen. Additionally, we validated UNC50. Thus, although the screening strategy may fail to identify all required factors, novel hits confirmed through a secondary screen likely play important roles in toxin trafficking/cytotoxicity. As additional hits in our screen are analyzed in the future, it is likely that obtained results will substantially enhance our understanding of the means by which STx1 and STx2 intoxicate cells and contribute toward the development of rational drug design strategies to selectively block retrograde toxin transport. A related issue is the caveat that functional and mechanistic analy-ses of hits remain challenging, which prevents high-throughput screens from having an immediate transformative effect on drug discovery. Nevertheless, identification of hits acts as the starting point for mechanistic studies, and recent technological advances such as the advent of CRISPR as a genome editing tool and the availability of improved small molecule inhibitors are expected to enhance the rate at which hits are functionally analyzed. Finally, as noted in the UNC50 is required for optimal transport. . . section of the Results, the fact that depletion of UNC50-affected trafficking of multiple cargoes suggests that it is unlikely to be the endosomal receptor for STx2B. It is possible that one of the other hits in the genome-wide screen functions as the endosomal STx2B receptor. However, the lack of saturation implies that the endosomal receptor for STx2B, if it exists, may also not be among the hits. Irrespective of the identification of the STx2B endosomal receptor, the arguments presented in this study imply that data obtained from the STx1 and STx2 genome-wide screens will likely have important impacts in the fields of STEC-induced disease, host pathogen interactions, and protein trafficking.

Complete loss of UNC50 profoundly inhibited early endosome-to-Golgi trafficking of STx2B. The underlying mechanism was the UNC50-dependent recruitment of GBF1 to the Golgi. The means by which association of GBF1 with Golgi membranes regulates trafficking events at the level of endosomes remains to be elucidated. Characterization of the recruitment of ARF-GEFs and clathrin adapters to STx2-positive endosomes in the presence or absence of GBF1 may be informative.

Localization of ARF-GEFs to specific membranes is important in ensuring compartment-specific coat protein recruitment. Rab1 and phosphatidylinositol 4-phosphate are known to be required for the recruitment of GBF1 to the Golgi (Donaldson

against giantin. (D) Quantification of the Pearson's coefficient for colocalization between STx2B and giantin from C (n = 25 cells per group). *, $P < 0.05$ for the comparison between WT cells at 60 min and *ΔUNC50* cells at 60 min by one-way ANOVA and Tukey-Kramer post hoc test. (E) Quantification of STx2B fluorescence intensities from C. Intensity of WT cells at 0 min was set to 100. Intensities of other groups were expressed relative to WT at 0 min ($n \geq 25$ cells per group). *, $P < 0.05$ for the difference between WT cells at 0 min and other groups using one-way ANOVA and Dunnett's post hoc test. (F) *ΔUNC50* cells were transfected with GFP-tagged Rab5. 1 d after transfection, transport of His-tagged STx2B was assayed. Cells were fixed 10 min after start of transport and imaged to detect STx2B using a polyclonal antibody against the His tag and GFP. Arrowheads show overlap between STx2B and GFP. (G) *ΔUNC50* cells were treated with leupeptin (100 µg/ml) and pepstatin (50 µg/ml) for 24 h or left untreated. After this, transport of STx2B was assayed. Cells were fixed at 0 min or 4 h after start of transport (0 min time-point is not depicted). STx2B was detected using a polyclonal antibody against the His tag. Golgi was demarcated using a monoclonal antibody against giantin. (H) Quantification of STx2B fluorescence intensities from G. For each treatment condition, intensity at 0 min was normalized to 100, and intensity at 4 h was expressed relative to 0 min (n = 25 cells per group). *, $P < 0.05$ by t test. (I) Transport of STx2B was assayed in *ΔUNC50* cells treated with leupeptin (100 µg/ml) and pepstatin (50 µg/ml) as described in G. Cells were fixed at the 4-h time point and imaged to detect STx2B, using the polyclonal anti-His antibody, and Lamp2, using a monoclonal antibody. Arrowheads show overlap between STx2B and Lamp2. (J) *ΔUNC50* cells were transfected with CRISPR-sensitive myc-tagged UNC50. 1 d after transfection, transport of STx2B was assayed. Cells were fixed at 0 or 60 min after start of transport and imaged to detect His and myc tags. Asterisks denote transfected cells. Bars: (C, G, and J) 25 µm; (F and I) 5 µm. (K) Quantification of STx2B fluorescence intensities from J. For each transfection condition, intensity at 0 min was set to 100, and intensity at 60 min was expressed relative to 0 min (n = 20 cells per group). *, $P < 0.05$ by t test. (L) Quantification of the Pearson's coefficient for colocalization between STx2B and myc-UNC50 at 0 or 60 min in transfected cells from J. The signal from myc-UNC50 demarcated the Golgi in transfected cells because in *ΔUNC50* cells, CRISPR-sensitive myc-UNC50 was enriched in the Golgi (Fig. 2, H–J; n = 25 cells per group). *, $P < 0.05$ by t test; error bars show means ± SEM.

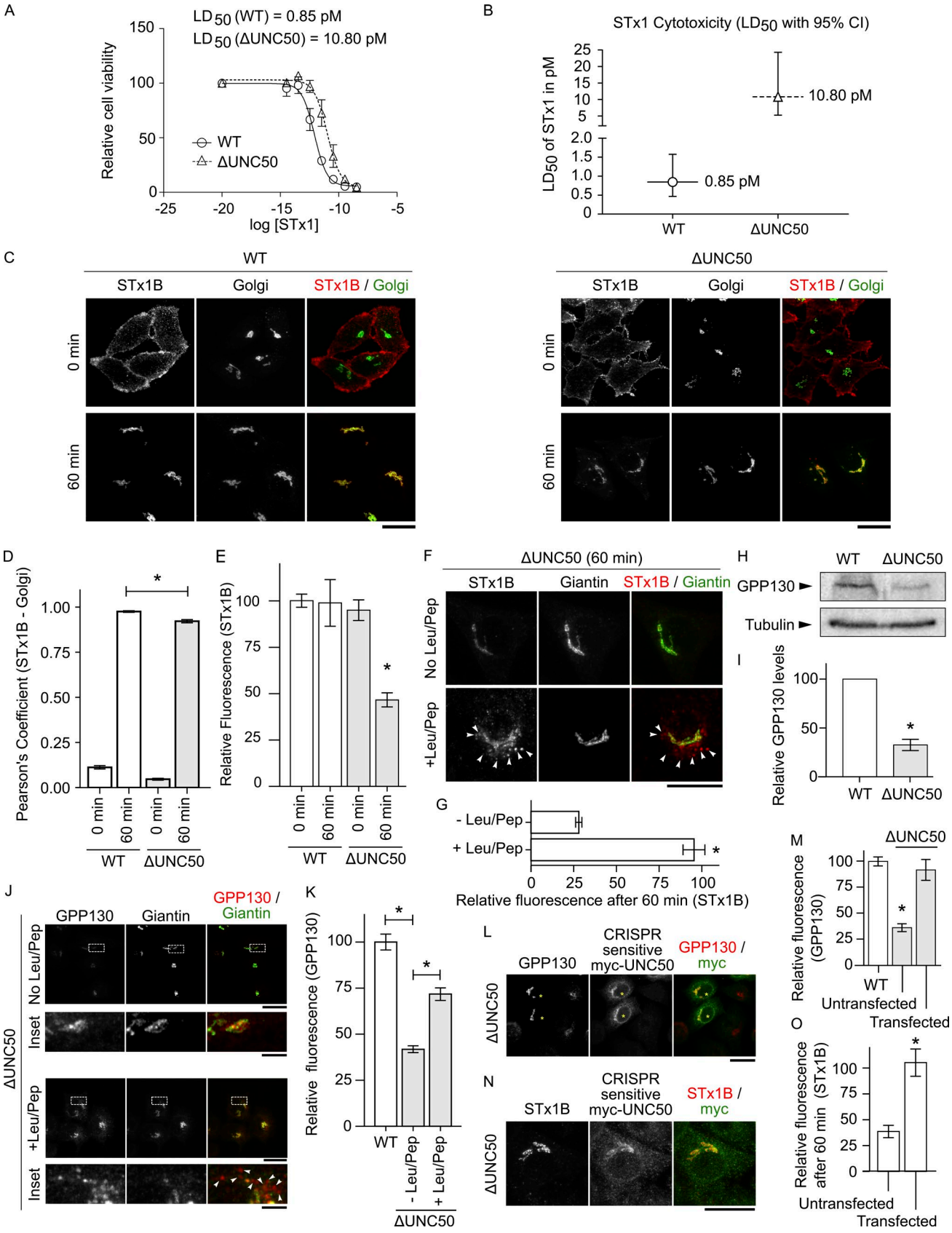

Figure 4. **UNC50 is required for the optimal transport of STx1 to the Golgi.** (A) Viability of WT or *ΔUNC50* cells exposed to indicated amounts of STx1 holotoxin for 16 h was assessed as described in Fig. 3 A (n = 3). (B) Depiction of the mean LD_{50} of STx1 from A with 95% confidence intervals (CIs). *, $P < 0.05$ by t test. (C) Trafficking of Alexa Fluor 555–labeled STx1B was assayed in WT or *ΔUNC50* cells. Cells were fixed at 0 or 60 min after start of transport. Golgi was demarcated using a monoclonal antibody against giantin. (D) Quantification of the Pearson's coefficient for colocalization between

and Jackson, 2011). UNC50 now emerges as another protein that plays an important role in regulating GBF1 localization. The process by which these factors cooperatively mediate membrane recruitment of GBF1 under physiological conditions as well as the consequences of changes in activities or levels of one or more of these factors in disease states (e.g., up-regulation of UNC50 in hepatocellular carcinoma; Fang et al., 2015) on GBF1 function is another important area of future research.

In *ΔUNC50* cells, a pool of STx1B still trafficked to the Golgi, implying that UNC50 is a differential regulator of cargo trafficking at the early endosome-to-Golgi transport step. Differences in the amount of STx1 and STx2 that were routed for lysosomal degradation in *ΔUNC50* cells may account for differences in the observed protective effects against each toxin. Moreover, loss of UNC50 also targeted the host STx1B endosomal receptor GPP130 for lysosomal degradation. These results are consistent with a study in *Caenorhabditis elegans* in which depletion of UNC50 led to lysosomal degradation of levamisole-sensitive acetylcholine receptor (Eimer et al., 2007). Overall, current evidence suggests that an important cellular function of UNC50 may be to regulate trafficking and localization of endogenous cargo proteins.

In conclusion, using an unbiased genome-wide siRNA screening strategy, we identified host genes required for STx1- and/or STx2-induced cytotoxicity and then elucidated the mechanism of action of UNC50. These results provide novel and critical insights into the biology of retrograde trafficking and STEC-induced disease.

Materials and methods

Cell culture

Unless otherwise specified, assays were performed using a HeLa cell subline that overexpressed globotriaosylceramide, the cell surface glycosphingolipid receptor for STx1B and STx2B. This cell line is referred to as WT throughout the study. We have extensively characterized the retrograde trafficking of STx1B and STx2B in this subline (Selyunin and Mukhopadhyay, 2015). For this study, cell culture was performed as described previously (Selyunin and Mukhopadhyay, 2015).

Primary genome-wide siRNA screen and data analyses

The screen was performed at the siRNA screening facility of M.D. Anderson Cancer Center. The human genome-wide siRNA library (GE Healthcare), which comprised pooled siRNAs targeting 21,067 predicted open reading frames such that each gene was targeted by four separate siRNAs, was used. The library is provided in 96-well plates, and the screen was performed in 384-well plates. For quality control, we included the following control conditions on every plate: wells with media only, wells with cells only, transfection with a nontargeting negative control siRNA (this was designed to control for nonspecific effects of siRNA transfection on viability), and transfection with a positive control siRNA that targeted polo-like kinase 1 (knockdown of polo-like kinase 1 induces apoptosis in cancer cells). Before initiation, ideal growth and transfection conditions as well as LD_{50} of STx1 and STx2 were established. Based on these optimization assays, we plated 800 HeLa cells per well and performed reverse transfection using Lipofectamine reagent (Invitrogen). 2 d after transfection, cells were treated with 0.1 pg/ml STx2 or 0.4 pg/ml STx1 for 72 h. Control conditions (media only, cells only, negative control siRNA, or positive control siRNA) were not exposed to any toxin. After toxin exposure, viability was assessed using the Cell Titer Blue Viability Assay (Promega). In brief, 100 µl of the reagent was introduced into each well containing 100 µl of media. The plates were placed on a shaker for 3 min to promote complete lysis of the cells, and luminescence intensity was determined using a PHERAstar plate reader (BMG LabTech). The screen was performed in triplicate for each toxin.

We analyzed the data using the following steps for each toxin. On each 384-well plate, we expressed the viability of siRNA-exposed and toxin-treated cells as a percentage of the viability of cells that were transfected with the negative control siRNA and not exposed to the toxin. Use of plate-specific controls was important to ensure results were not confounded by plate-to-plate variations. After this, for each knockdown, we calculated the median viability from the triplicate. Next, we calculated the mean of the median viability for all genes in the screen. This was 43 ± 11% (mean ± SD) for STx1 and 42 ± 10% (mean ± SD) for STx2. Finally, we classified genes in which, after knockdown and toxin exposure, viability was two SDs greater than the mean of the median of all genes in the screen as hits (i.e., >65% on the STx1 screen and >62% on the STx2 screen; these genes had a z score >2).

STx1B and giantin from C (n = 25 cells per group). *, P < 0.05 for the comparison between WT cells at 60 min and *ΔUNC50* cells at 60 min by one-way ANOVA and Tukey-Kramer post hoc test. (E) Quantification of STx1B fluorescence intensities from C. Intensity of WT cells at 0 min was set to 100. Intensities of other groups were expressed relative to WT at 0 min (n = 25 cells per group). *, P < 0.05 for the difference between WT cells at 0 min and other groups using one-way ANOVA and Dunnett's post hoc test. (F) *ΔUNC50* cells were treated with leupeptin (100 µg/ml) and pepstatin (50 µg/ml) for 24 h or left untreated. Transport of fluorescently labeled STx1B was then assayed. Cells were fixed at 0 or 60 min after start of transport (0-min time point is not depicted). Golgi was demarcated using a monoclonal antibody against giantin. (G) Quantification of STx1B fluorescence intensities from F. For each treatment condition, intensity at 0 min was normalized to 100, and intensity at 60 min was expressed relative to 0 min ($n \geq 25$ cells per group). *, P < 0.05 by t test. (H) Immunoblot analyses were performed using lysates prepared from WT or *ΔUNC50* cells to detect GPP130, using a polyclonal antibody, or tubulin, using a monoclonal antibody. (I) Quantification of GPP130 levels normalized to tubulin from H (n = 3). *, P < 0.05 by t test. (J) *ΔUNC50* cells were treated with or without leupeptin (100 µg/ml) and pepstatin (50 µg/ml) for 24 h and stained to detect GPP130, using a monoclonal antibody, and giantin, using a polyclonal antibody. Arrowheads show GPP130 in cytoplasmic punctae. Dotted boxes mark insets. (K) Quantification of GPP130 levels from J. Note that images for WT cells are not depicted in J. For quantification, fluorescence intensity in WT cells was set to 100, and intensities in *ΔUNC50* cells were expressed relative to WT ($n \geq 25$ cells per group). *, P < 0.05 for the difference in GPP130 levels between indicated groups using one-way ANOVA and Tukey-Kramer post hoc test. (L) *ΔUNC50* cells were transfected with CRISPR-sensitive myc-tagged UNC50. 1 d after transfection, cells were fixed and imaged to detect GPP130, using a polyclonal antibody, and the myc tag. Asterisks denote transfected cells. (M) Quantification of GPP130 levels from L. Note that images for WT cells, which were not transfected with the myc-UNC50 plasmid, are not depicted in L. For quantification, fluorescence intensity in WT cells was set to 100, and intensities in *ΔUNC50* cells were expressed relative to WT ($n \geq 15$ cells per group). *, P < 0.05 for the difference between WT and other groups using one-way ANOVA and Dunnett's post hoc test. (N) *ΔUNC50* cells were transfected with CRISPR-sensitive myc-tagged UNC50. 1 d after transfection, transport of fluorescently labeled STx1B was assayed. Cells were fixed at 0 or 60 min after start of transport (the 0-min time point is not depicted) and imaged to detect STx1B and myc. Bars: (C, F, J [main images], L, and N) 25 µm; (J, insets) 5 µm. (O) Quantification of STx1B fluorescence intensities from N. For each transfection condition, intensity at 0 min was normalized to 100, and intensity at 60 min was expressed relative to 0 min (n = 15 cells per group). *, P < 0.05 by t test; error bars show means ± SEM.

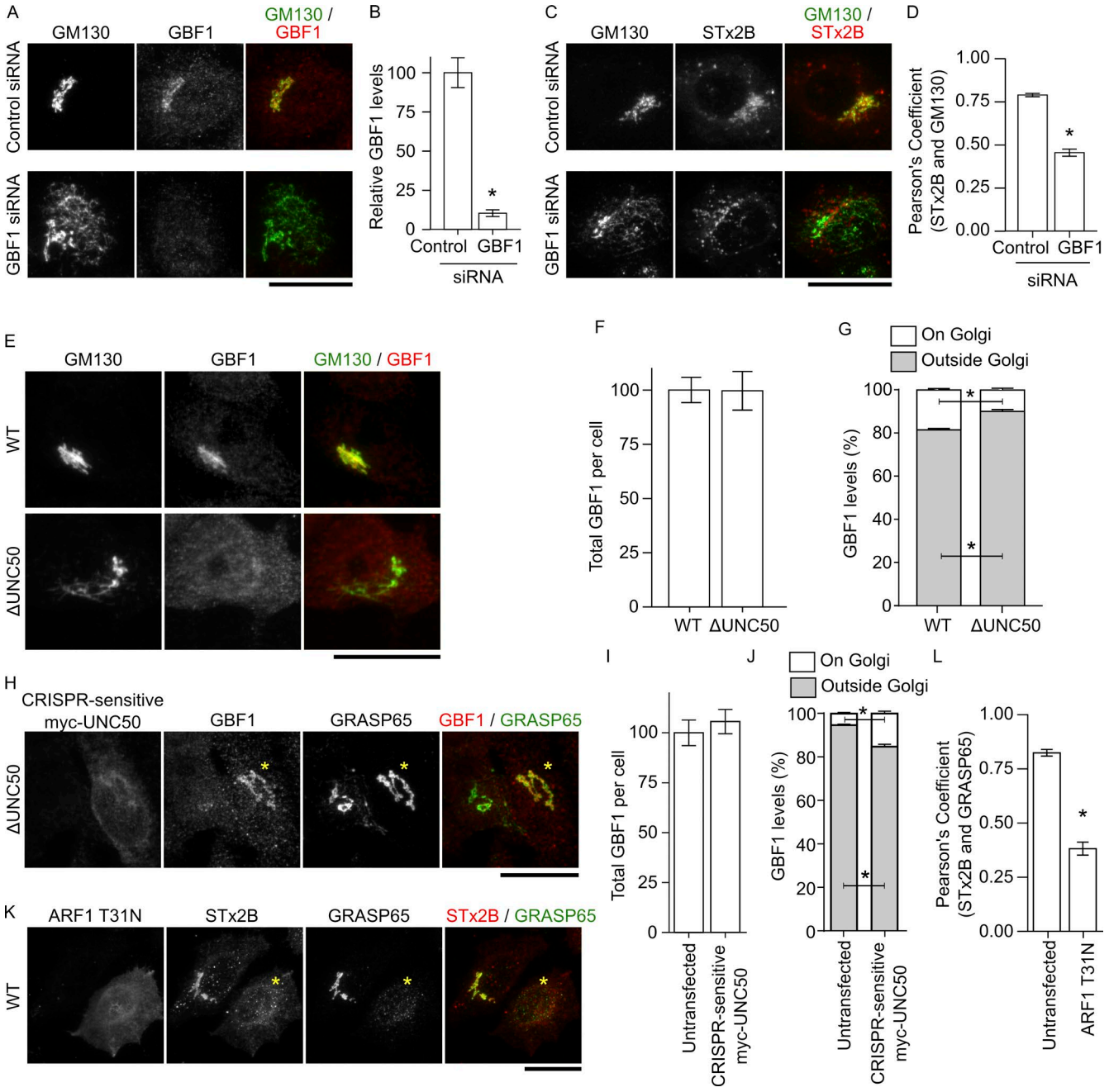

Figure 5. **UNC50 mediates recruitment of GBF1 to the Golgi apparatus.** (A) WT cells were transfected with control or anti-GBF1 siRNAs. After 48 h, cells were imaged to detect GM130 and GBF1. (B) Quantification of GBF1 fluorescence intensities from A. Intensity in cells transfected with control siRNA was normalized to 100 (n = 15 cells). *, P < 0.05 by t test. (C) Trafficking of His-tagged STx2B was assayed in cells transfected with control or anti-GBF1 siRNAs for 48 h. Cells were fixed 60 min after start of transport. STx2B was detected using a polyclonal antibody against the His tag. Golgi was demarcated using a monoclonal antibody against GM130. (D) Quantification of the Pearson's coefficient for colocalization between STx2B and GM130 from C (n = 15 cells). *, P < 0.05 by t test. (E) WT or *ΔUNC50* cells were fixed, and endogenous GM130 and GBF1 were detected using monoclonal and polyclonal antibodies, respectively. (F) Quantification of GBF1 levels from E. Intensity in WT cells was normalized to 100 (n = 15 cells). (G) Quantification of the relative intracellular distribution of GBF1 from E. Signal for GM130 was used to delineate the Golgi (n = 25 cells). *, P < 0.05 between indicated groups using one-way ANOVA and Tukey-Kramer post hoc test. (H) *ΔUNC50* cells were transfected with CRISPR-sensitive myc-UNC50 for 24 h. After this, cultures were fixed and stained to detect endogenous GBF1, GRASP65, and the myc tag. Asterisks denote transfected cells. (I) Quantification of GBF1 levels from H. Intensity in untransfected cells was normalized to 100 (n = 15 cells). (J) Quantification of the relative intracellular distribution of GBF1 from H. Golgi was demarcated using the signal for GRASP65 (n = 15 cells). *, P < 0.05 between indicated groups using one-way ANOVA and Tukey-Kramer post hoc test. (K) WT cells were transfected with HA-tagged dominant-negative $ARF1_{T31N}$ for 24 h. After this, transport of His-STx2B was assayed. Cells were fixed 60 min after start of transport. ARF1 was detected using a monoclonal antibody against the HA tag, STx2B was detected using a polyclonal antibody against the His tag, and GRASP65 was detected using a polyclonal antibody. Asterisks denote transfected cells. Bars, 25 µm. (L) Quantification of the Pearson's coefficient for colocalization between STx2B and GRASP65 from K (n = 15 cells). *, P < 0.05 by t test; error bars show means ± SEM.

Secondary screen and data analyses

The secondary screen was also performed at the siRNA screening facility of M.D. Anderson Cancer Center. For each selected primary screen hit, the siRNA pool was deconvoluted, and each hit was independently targeted using four separate siRNAs. Further processing, including positive control and negative control siRNAs used, exposure to STx2 (0.1 pg/ml, which is the LD_{50} of STx2), and assessment of cell viability was done exactly as described for the primary screen. Each siRNA transfection was performed at least in triplicate. After this, identical to the primary screen, we expressed the viability of siRNA- and toxin-treated cells as a percentage of the viability of cells transfected with the negative control siRNA and not exposed to the toxin. We then calculated the median viability for each siRNA knockdown from replicates. Finally, we considered genes for which after knockdown with at least two siRNAs, median viability after toxin exposure was >62% (the cutoff necessary to be considered a hit in the primary STx2 screen) as validated hits. Note that, as cells were treated with the LD_{50} of STx2, arguably, it was possible to consider any gene with viability >50% as validated. However, we used a higher (>62%) viability cutoff to reduce the risk of performing time-consuming functional assays on false-positive hits; if at least two siRNAs gave a level of protection similar to the siRNA pool used in the primary screen, the likelihood of a false positive was reduced.

Generation of ΔUNC50 HeLa cells

We generated *ΔUNC50* cells using a lentiviral-based CRISPR system. The lentiviral transfer plasmid (57818; Addgene; Heckl et al., 2014) coexpressed the guide RNA and Cas9. The sequence of the guide RNA was 5′-AATCTATGAGTACAACCCAA-3′. The targeted complementary sequence in the *UNC50* gene included nucleotides 345–364, which code for amino acids 114–122 in exon 2. We used HEK293T cells and a third-generation packaging system to produce lentivirus. Cotransfection of the packaging plasmids pRSV-Rev and pRRE, the envelope plasmid pHCMV-G, and the transfer plasmid was done as follows. HEK293T cells were plated in 10-cm plates such that 24 h after plating, the culture was ∼80–90% confluent. Before transfection, the media was replaced with 5.5 ml of fresh DMEM/F12 (Corning) supplemented with 10% FBS (Atlanta Biologicals). There were no antibiotics in the media. After this, a transfection mix was prepared that contained 1.5 ml of Opti-MEM (Thermo Fisher Scientific), 45 µl of TransIT-2020 transfection reagent (Mirus Bio), and 4 µg of each plasmid. The transfection mixture was gently mixed, incubated at room temperature for 30 min, and added to cells. After 40–48 h of transfection, the media was removed and filtered through a 0.45-µm polyvinylidene difluoride filter. Then, 30 µg of polybrene (Santa Cruz Biotechnology, Inc.) was added to the filtered media, and ∼3 ml of the mixture was dispended into a 35-mm dish. Approximately 1 ml of freshly trypsinized HeLa cells that were the lentivirus target were plated into the 35-mm dish at a concentration of ∼300,000 cells/ml. Note that these cells overexpressed globotriaosylceramide. After 24 h of infection, cells were passaged and now maintained in DMEM/F12 containing 10% FBS and supplemented with 100 U/ml penicillin and 100 µg/ml streptomycin (Corning). Finally, single-cell clones were generated, selected, and expanded.

Genomic DNA was extracted from these clones using Puregene Core kit A (QIAGEN). For sequencing, we PCR amplified an ∼250–base pair region around the locus targeted by the CRISPR system, inserted the PCR-amplified region into pCR4-TOPO vector using the TopoTA cloning kit (Thermo Fisher Scientific), and for each HeLa cell clone, sequenced 10–12 bacterial colonies.

Plasmid constructs and transient DNA transfections

Plasmids for generating lentivirus are described in the previous section. Myc-DDK-GBF1 plasmid (RC235341) was from OriGene. HA-tagged $ARF1_{T31N}$ plasmid was from Addgene (10833; Addgene; Furman et al., 2002). We previously described the untagged STx1B and Rab5-GFP plasmids (Selyunin and Mukhopadhyay, 2015). CRISPR-sensitive myc-tagged full-length UNC50 was generated as follows. RNA was extracted from HeLa cells and reverse transcribed to cDNA as described previously (Leyva-Illades et al., 2014). The *UNC50* gene was amplified using the following primers: forward, 5′-AACTCGAGATGGAACAAAAACTCATCTCAGAAGAGGATCTGATGTTACCGAGTACTTCAG-3′; and reverse, 5′-AAGGATCCTTATTTCACTCTGTACTTATAGAAAGAAC-3′. PCR conditions were as follows: 94°C for 5 min, 30 cycles of 94°C for 30 s, 55°C for 30 s, 72°C for 1 min, and 72°C for 10 min. The PCR product was digested using XhoI and BamHI enzymes (New England Biolabs, Inc.) and ligated into pEGFP-N3 vector; there was a stop codon before the start of the GFP coding sequence. The CRISPR-resistant construct was generated by introducing a silent mutation in the protospacer-adjacent motif sequence that precedes the target DNA sequence in the CRISPR-sensitive construct described above. The silent mutation was introduced using QuikChange as described previously (Selyunin and Mukhopadhyay, 2015); primers consisted of forward, 5′-CTTTGAGACAATAAAGCTTCTATTGTGGGTTGTACTCATAGATTG-3′; and the reverse primer, which was the inverse complement of the forward primer. GFP-tagged SLC30A10 plasmid was generated by amplifying the SLC30A10 sequence from the previously described FLAG-SLC30A10 plasmid (Leyva-Illades et al., 2014; Zogzas et al., 2016) and inserting it into pEGFP-N3 vector. Plasmids were transfected using the JetPEI transfection reagent as described previously (Selyunin and Mukhopadhyay, 2015).

siRNA transfections to deplete GBF1

siRNA transfections were performed as described previously (Mukhopadhyay and Linstedt, 2011; Leyva-Illades et al., 2014; Selyunin and Mukhopadhyay, 2015). The control siRNA does not target any human gene and has been extensively characterized by us (Mukhopadhyay and Linstedt, 2011; Leyva-Illades et al., 2014; Selyunin and Mukhopadhyay, 2015). The siRNA against GBF1 targeted the sequence 5′-CGAAATGCCCGATGGAGCA-3′ in the human *GBF1* gene and has been previously described (Szul et al., 2007).

RT-PCR

These were performed from cDNA generated from WT or *ΔUNC50* cells. Primers used were as follows: for amplification of an ∼170–base pair fragment from sequences upstream of the region targeted by the CRISPR, forward, 5′-CAGATGCTCTACCTGTTCACATCCC-3′; and reverse, 5′-GAATCCCATGTCCAGCACAAAGCC-3′; and for amplification of an ∼140–base pair fragment from sequences downstream of the region targeted by the CRISPR, forward, 5′-GTTGGCTATTATATCTATGTAACTTTCCTGGG-3′; and reverse, 5′-GGGTGAAGTTCCATCCCAGTGC-3′. PCR conditions were as follows: 94°C for 5 min, 30 cycles of 94°C for 30 s, 57°C for 30 s, 72°C for 1 min, and 72°C for 10 min.

Protein purification, labeling, and transport assays

Purification and labeling of untagged STx1B with Alexa Fluor 555 (Thermo Fisher Scientific) was done as described previously (Selyunin and Mukhopadhyay, 2015). His-tagged STx2B was obtained from BEI Resources. Transport assays using untagged STx1B or His-tagged STx2B were performed exactly as described previously (Selyunin and Mukhopadhyay, 2015).

Viability assays

WT or *ΔUNC50* HeLa cells were exposed to indicated doses of STx1 or STx2 for 16 h. The toxins were obtained from BEI Resources. Viability

was assessed using the (3-(4,5-dimethylthiazol-2-yl)-2,5-diphenyltetrazolium bromide 3-4-5 (MTT) reagent as described previously (Leyva-Illades et al., 2014; Zogzas et al., 2016).

Antibodies

Monoclonal antibodies against the myc tag and GM130 were from Sigma-Aldrich and BD, respectively. Polyclonal antibody against GBF1 was from Abcam. We have previously described other antibodies used in this study (polyclonal antibodies against the His tag, calnexin, and GRASP65, monoclonal and polyclonal antibodies against GPP130, monoclonal and polyclonal antibodies against giantin, and monoclonal antibodies against tubulin, the HA tag, and Lamp2; Mukhopadhyay et al., 2010; Mukhopadhyay and Linstedt, 2011, 2012; Leyva-Illades et al., 2014; Selyunin and Mukhopadhyay, 2015; Zogzas et al., 2016).

Immunofluorescence, microscopy, and image analyses

These were performed exactly as described previously (Selyunin and Mukhopadhyay, 2015). To summarize details of the microscope in this study, we used a sweptfield confocal microscope equipped with a four-line high-power laser launch and a 100× 1.45 NA oil immersion objective (Nikon). An iXon3 X3 DU897 electron-multiplying charge-coupled device camera (Andor Technology) was used for image capture. All images were captured as z stacks with 0.2-µm spacing between individual frames. Images depicted in the figures are maximum-intensity projections of the stacks.

All analyses were performed using ImageJ (National Institutes of Health) as described previously (Selyunin and Mukhopadhyay, 2015).

Immunoblot analyses

Cells were lysed in buffer containing 150 mM NaCl, 1% NP-40 (Sigma-Aldrich), 0.1% sodium dodecyl sulfate, and 50 mM Tris, pH 8.0. Whole-cell lysates were centrifuged at 14,000 *g* for 20 min at 4°C. The supernatant was used for immunoblot analyses as described previously (Leyva-Illades et al., 2014). Immunoblots were quantified using ImageJ.

Statistical analyses

Detailed methodology used to analyze data from the genome-wide siRNA screen is described in the Primary genome-wide siRNA screen… section above. For other statistical analyses, we used Prism6 software (GraphPad Software). All experiments were repeated at least three times independently. Comparisons between two groups were performed using Student's *t* test assuming equal variances. Comparisons between multiple groups at the same time were performed using one-way ANOVA followed by Dunnett's or Tukey-Kramer post hoc tests. Nonparametric statistics were used to calculate LD_{50} of STx1 and STx2. For all analyses, $P < 0.05$ was considered to be statistically significant. Asterisks in graphs, where present, denote statistically significant differences.

Online supplemental material

Table S1 shows data from the STx1 primary screen. Table S2 shows data from the STx2 primary screen. Table S3 provides a list of primary screen hits that were specific for STx1 (STx1-unique hits), specific for STx2 (STx2-unique hits), or common for both toxins. Table S4 provides a list of primary screen hits predicted to localize to endosomes/Golgi. Table S5 presents data from the secondary screen.

Acknowledgments

This work was supported by the National Institutes of Health/National Institute of Allergy and Infectious Diseases grant R21-AI123608 to S. Mukhopadhyay and an American Heart Association postdoctoral fellowship 16POST30240016 to A.S. Selyunin.

The authors declare no competing financial interests.

Author contributions: L.R. Iles and G. Bartholomeusz performed the siRNA screens. A.S. Selyunin performed all other experiments, analyzed data, generated figures, and assisted in writing the manuscript. S. Mukhopadhyay conceived the project, analyzed data, and wrote the manuscript.

Submitted: 3 April 2017
Revised: 6 July 2017
Accepted: 2 August 2017

References

Bachert, C., T.H. Lee, and A.D. Linstedt. 2001. Lumenal endosomal and Golgi-retrieval determinants involved in pH-sensitive targeting of an early Golgi protein. *Mol. Biol. Cell.* 12:3152–3160. http://dx.doi.org/10.1091/mbc.12.10.3152

Bassik, M.C., M. Kampmann, R.J. Lebbink, S. Wang, M.Y. Hein, I. Poser, J. Weibezahn, M.A. Horlbeck, S. Chen, M. Mann, et al. 2013. A systematic mammalian genetic interaction map reveals pathways underlying ricin susceptibility. *Cell.* 152:909–922. http://dx.doi.org/10.1016/j.cell.2013.01.030

Beddoe, T., A.W. Paton, J. Le Nours, J. Rossjohn, and J.C. Paton. 2010. Structure, biological functions and applications of the AB5 toxins. *Trends Biochem. Sci.* 35:411–418. http://dx.doi.org/10.1016/j.tibs.2010.02.003

Boerlin, P., S.A. McEwen, F. Boerlin-Petzold, J.B. Wilson, R.P. Johnson, and C.L. Gyles. 1999. Associations between virulence factors of Shiga toxin-producing *Escherichia coli* and disease in humans. *J. Clin. Microbiol.* 37:497–503.

Bonifacino, J.S. 2004. The GGA proteins: adaptors on the move. *Nat. Rev. Mol. Cell Biol.* 5:23–32. http://dx.doi.org/10.1038/nrm1279

Chantalat, S., R. Courbeyrette, F. Senic-Matuglia, C.L. Jackson, B. Goud, and A. Peyroche. 2003. A novel Golgi membrane protein is a partner of the ARF exchange factors Gea1p and Gea2p. *Mol. Biol. Cell.* 14:2357–2371. http://dx.doi.org/10.1091/mbc.E02-10-0693

Donaldson, J.G., and C.L. Jackson. 2011. ARF family G proteins and their regulators: roles in membrane transport, development and disease. *Nat. Rev. Mol. Cell Biol.* 12:362–375. http://dx.doi.org/10.1038/nrm3117

Eimer, S., A. Gottschalk, M. Hengartner, H.R. Horvitz, J. Richmond, W.R. Schafer, and J.L. Bessereau. 2007. Regulation of nicotinic receptor trafficking by the transmembrane Golgi protein UNC-50. *EMBO J.* 26:4313–4323. http://dx.doi.org/10.1038/sj.emboj.7601858

Fang, Z., L. Zhou, S. Jiang, L. Cao, and L. Yu. 2015. UNC50 prompts G1/S transition and proliferation in HCC by regulation of epidermal growth factor receptor trafficking. *PLoS One.* 10:e0119338. http://dx.doi.org/10.1371/journal.pone.0119338

Fuchs, E., A.K. Haas, R.A. Spooner, S. Yoshimura, J.M. Lord, and F.A. Barr. 2007. Specific Rab GTPase-activating proteins define the Shiga toxin and epidermal growth factor uptake pathways. *J. Cell Biol.* 177:1133–1143. http://dx.doi.org/10.1083/jcb.200612068

Furman, C., S.M. Short, R.R. Subramanian, B.R. Zetter, and T.M. Roberts. 2002. DEF-1/ASAP1 is a GTPase-activating protein (GAP) for ARF1 that enhances cell motility through a GAP-dependent mechanism. *J. Biol. Chem.* 277:7962–7969. http://dx.doi.org/10.1074/jbc.M109149200

Heckl, D., M.S. Kowalczyk, D. Yudovich, R. Belizaire, R.V. Puram, M.E. McConkey, A. Thielke, J.C. Aster, A. Regev, and B.L. Ebert. 2014. Generation of mouse models of myeloid malignancy with combinatorial genetic lesions using CRISPR-Cas9 genome editing. *Nat. Biotechnol.* 32:941–946. http://dx.doi.org/10.1038/nbt.2951

Jackson, C.L., and S. Bouvet. 2014. Arfs at a glance. *J. Cell Sci.* 127:4103–4109. http://dx.doi.org/10.1242/jcs.144899

Kavaliauskiene, S., A.B. Dyve Lingelem, T. Skotland, and K. Sandvig. 2017. Protection against Shiga toxins. *Toxins (Basel).* 9:44. http://dx.doi.org/10.3390/toxins9020044

Leyva-Illades, D., P. Chen, C.E. Zogzas, S. Hutchens, J.M. Mercado, C.D. Swaim, R.A. Morrisett, A.B. Bowman, M. Aschner, and S. Mukhopadhyay. 2014. SLC30A10 is a cell surface-localized manganese efflux transporter, and parkinsonism-causing mutations block its intracellular trafficking and efflux activity. *J. Neurosci.* 34:14079–14095. http://dx.doi.org/10.1523/JNEUROSCI.2329-14.2014

Linstedt, A.D., A. Mehta, J. Suhan, H. Reggio, and H.P. Hauri. 1997. Sequence and overexpression of GPP130/GIMPc: evidence for saturable pH-

sensitive targeting of a type II early Golgi membrane protein. *Mol. Biol. Cell.* 8:1073–1087. http://dx.doi.org/10.1091/mbc.8.6.1073

Lowery, J., T. Szul, M. Styers, Z. Holloway, V. Oorschot, J. Klumperman, and E. Sztul. 2013. The Sec7 guanine nucleotide exchange factor GBF1 regulates membrane recruitment of BIG1 and BIG2 guanine nucleotide exchange factors to the trans-Golgi network (TGN). *J. Biol. Chem.* 288:11532–11545. http://dx.doi.org/10.1074/jbc.M112.438481

Mallard, F., C. Antony, D. Tenza, J. Salamero, B. Goud, and L. Johannes. 1998. Direct pathway from early/recycling endosomes to the Golgi apparatus revealed through the study of shiga toxin B-fragment transport. *J. Cell Biol.* 143:973–990. (published correction appears in *J. Cell Biol.* 1999. 145:1521) http://dx.doi.org/10.1083/jcb.143.4.973

Manolea, F., A. Claude, J. Chun, J. Rosas, and P. Melançon. 2008. Distinct functions for Arf guanine nucleotide exchange factors at the Golgi complex: GBF1 and BIGs are required for assembly and maintenance of the Golgi stack and trans-Golgi network, respectively. *Mol. Biol. Cell.* 19:523–535. http://dx.doi.org/10.1091/mbc.E07-04-0394

Matsushiro, A., K. Sato, H. Miyamoto, T. Yamamura, and T. Honda. 1999. Induction of prophages of enterohemorrhagic *Escherichia coli* O157:H7 with norfloxacin. *J. Bacteriol.* 181:2257–2260.

McGannon, C.M., C.A. Fuller, and A.A. Weiss. 2010. Different classes of antibiotics differentially influence shiga toxin production. *Antimicrob. Agents Chemother.* 54:3790–3798. http://dx.doi.org/10.1128/AAC.01783-09

Moreau, D., P. Kumar, S.C. Wang, A. Chaumet, S.Y. Chew, H. Chevalley, and F. Bard. 2011. Genome-wide RNAi screens identify genes required for Ricin and PE intoxications. *Dev. Cell.* 21:231–244. http://dx.doi.org/10.1016/j.devcel.2011.06.014

Mukhopadhyay, S., and A.D. Linstedt. 2011. Identification of a gain-of-function mutation in a Golgi P-type ATPase that enhances Mn^{2+} efflux and protects against toxicity. *Proc. Natl. Acad. Sci. USA.* 108:858–863. http://dx.doi.org/10.1073/pnas.1013642108

Mukhopadhyay, S., and A.D. Linstedt. 2012. Manganese blocks intracellular trafficking of Shiga toxin and protects against Shiga toxicosis. *Science.* 335:332–335. http://dx.doi.org/10.1126/science.1215930

Mukhopadhyay, S., and A.D. Linstedt. 2013. Retrograde trafficking of AB_5 toxins: mechanisms to therapeutics. *J. Mol. Med. (Berl.).* 91:1131–1141. http://dx.doi.org/10.1007/s00109-013-1048-7

Mukhopadhyay, S., C. Bachert, D.R. Smith, and A.D. Linstedt. 2010. Manganese-induced trafficking and turnover of the cis-Golgi glycoprotein GPP130. *Mol. Biol. Cell.* 21:1282–1292. http://dx.doi.org/10.1091/mbc.E09-11-0985

Mukhopadhyay, S., B. Redler, and A.D. Linstedt. 2013. Shiga toxin-binding site for host cell receptor GPP130 reveals unexpected divergence in toxin-trafficking mechanisms. *Mol. Biol. Cell.* 24:2311–2318. http://dx.doi.org/10.1091/mbc.E13-01-0057

Natarajan, R., and A.D. Linstedt. 2004. A cycling cis-Golgi protein mediates endosome-to-Golgi traffic. *Mol. Biol. Cell.* 15:4798–4806. http://dx.doi.org/10.1091/mbc.E04-05-0366

Nataro, J.P. 2006. P.L. *In* Oski's Paediatrics: Principles and Practice. F.R. J.A. McMillan, C.D. DeAngelis, and M. Douglas Jones Jr., editors. Lippincott Williams and Wilkins, Philadelphia. 1063–1068.

Ochoa, T.J., and T.G. Cleary. 2006. Shigellosis. *In* Oski's Paediatrics: Principle and Practice. J.A. McMillan, R.D. Feigin, C. DeAngelis, and M.D. Jones Jr., editors. Lippincott, Williams & Wilkins, Philadelphia, PA. 1116–1120.

Saenz, J.B., T.A. Doggett, and D.B. Haslam. 2007. Identification and characterization of small molecules that inhibit intracellular toxin transport. *Infect. Immun.* 75:4552–4561. http://dx.doi.org/10.1128/IAI.00442-07

Sáenz, J.B., W.J. Sun, J.W. Chang, J. Li, B. Bursulaya, N.S. Gray, and D.B. Haslam. 2009. Golgicide A reveals essential roles for GBF1 in Golgi assembly and function. *Nat. Chem. Biol.* 5:157–165. http://dx.doi.org/10.1038/nchembio.144

Selyunin, A.S., and S. Mukhopadhyay. 2015. A conserved structural motif mediates retrograde trafficking of Shiga toxin types 1 and 2. *Traffic.* 16:1270–1287. http://dx.doi.org/10.1111/tra.12338

Shen, X., K.F. Xu, Q. Fan, G. Pacheco-Rodriguez, J. Moss, and M. Vaughan. 2006. Association of brefeldin A-inhibited guanine nucleotide-exchange protein 2 (BIG2) with recycling endosomes during transferrin uptake. *Proc. Natl. Acad. Sci. USA.* 103:2635–2640. http://dx.doi.org/10.1073/pnas.0510599103

Shiba, Y., W. Römer, G.A. Mardones, P.V. Burgos, C. Lamaze, and L. Johannes. 2010. AGAP2 regulates retrograde transport between early endosomes and the TGN. *J. Cell Sci.* 123:2381–2390. http://dx.doi.org/10.1242/jcs.057778

Shin, H.W., N. Morinaga, M. Noda, and K. Nakayama. 2004. BIG2, a guanine nucleotide exchange factor for ADP-ribosylation factors: Its localization to recycling endosomes and implication in the endosome integrity. *Mol. Biol. Cell.* 15:5283–5294. http://dx.doi.org/10.1091/mbc.E04-05-0388

Stechmann, B., S.K. Bai, E. Gobbo, R. Lopez, G. Merer, S. Pinchard, L. Panigai, D. Tenza, G. Raposo, B. Beaumelle, et al. 2010. Inhibition of retrograde transport protects mice from lethal ricin challenge. *Cell.* 141:231–242. http://dx.doi.org/10.1016/j.cell.2010.01.043

Strockbine, N.A., M.P. Jackson, L.M. Sung, R.K. Holmes, and A.D. O'Brien. 1988. Cloning and sequencing of the genes for Shiga toxin from Shigella dysenteriae type 1. *J. Bacteriol.* 170:1116–1122. http://dx.doi.org/10.1128/jb.170.3.1116-1122.1988

Szul, T., R. Grabski, S. Lyons, Y. Morohashi, S. Shestopal, M. Lowe, and E. Sztul. 2007. Dissecting the role of the ARF guanine nucleotide exchange factor GBF1 in Golgi biogenesis and protein trafficking. *J. Cell Sci.* 120:3929–3940. http://dx.doi.org/10.1242/jcs.010769

Tesh, V.L., J.A. Burris, J.W. Owens, V.M. Gordon, E.A. Wadolkowski, A.D. O'Brien, and J.E. Samuel. 1993. Comparison of the relative toxicities of Shiga-like toxins type I and type II for mice. *Infect. Immun.* 61:3392–3402.

Tewari, R., T. Jarvela, and A.D. Linstedt. 2014. Manganese induces oligomerization to promote down-regulation of the intracellular trafficking receptor used by Shiga toxin. *Mol. Biol. Cell.* 25:3049–3058. http://dx.doi.org/10.1091/mbc.E14-05-1003

Tewari, R., C. Bachert, and A.D. Linstedt. 2015. Induced oligomerization targets Golgi proteins for degradation in lysosomes. *Mol. Biol. Cell.* 26:4427–4437. http://dx.doi.org/10.1091/mbc.E15-04-0207

Tokuda, N., S. Numata, X. Li, T. Nomura, M. Takizawa, Y. Kondo, Y. Yamashita, N. Hashimoto, T. Kiyono, T. Urano, et al. 2013. β4GalT6 is involved in the synthesis of lactosylceramide with less intensity than β4GalT5. *Glycobiology.* 23:1175–1183. http://dx.doi.org/10.1093/glycob/cwt054

Walterspiel, J.N., S. Ashkenazi, A.L. Morrow, and T.G. Cleary. 1992. Effect of subinhibitory concentrations of antibiotics on extracellular Shiga-like toxin I. *Infection.* 20:25–29. http://dx.doi.org/10.1007/BF01704889

Zhang, X., A.D. McDaniel, L.E. Wolf, G.T. Keusch, M.K. Waldor, and D.W. Acheson. 2000. Quinolone antibiotics induce Shiga toxin-encoding bacteriophages, toxin production, and death in mice. *J. Infect. Dis.* 181:664–670. http://dx.doi.org/10.1086/315239

Zogzas, C.E., M. Aschner, and S. Mukhopadhyay. 2016. Structural elements in the transmembrane and cytoplasmic domains of the metal transporter SLC30A10 are required for its manganese efflux activity. *J. Biol. Chem.* 291:15940–15957. http://dx.doi.org/10.1074/jbc.M116.726935

Zolov, S.N., and V.V. Lupashin. 2005. Cog3p depletion blocks vesicle-mediated Golgi retrograde trafficking in HeLa cells. *J. Cell Biol.* 168:747–759. http://dx.doi.org/10.1083/jcb.200412003